Protist 177 (2025) 126099

Contents lists available at ScienceDirect

Protist

journal homepage: www.elsevier.de/protis

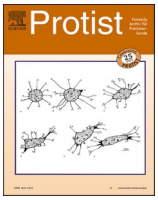

Original article

Morphology and phylogeny of *Prorocentrum venetum* Tolomio & Cavolo (Dinophyceae)

Daniel Grzebyk [a,*], Mona Hoppenrath [b], Urban Tillmann [c]

[a] MARBEC, Univ Montpellier, CNRS, Ifremer, IRD, Montpellier, France
[b] Senckenberg am Meer, German Centre for Marine Biodiversity Research (DZMB), Südstrand 44, 26382 Wilhelmshaven, Germany
[c] Alfred Wegener Institute for Polar and Marine Research, Am Handelshafen 12, 27570 Bremerhaven, Germany

ARTICLE INFO

Editor Name: Ellen Nisbet

Keywords:
rDNA sequence
Morphology
Phylogeny
Taxonomy

ABSTRACT

Prorocentrum venetum was one of the first species of the genus *Prorocentrum* described by scanning electron microscopy by Tolomio and Cavolo in 1985. Since the first observation of the species in the Venice Lagoon (Italy) in summer 1981, it has not been reported again in published phytoplankton records of Mediterranean waters or elsewhere. Two strains were isolated from a French Mediterranean lagoon, which were morphologically identified as *P. venetum* by microscopy. Based on rDNA sequences (spanning the 18S to the D3 region of 28S rDNA), the phylogenetic analysis demonstrated that *P. venetum* belongs to the same clade as *Prorocentrum triestinum* and *Prorocentrum redfieldii*. The analysis of scanning electron micrographs provided an in-depth morphological description of the theca, particularly on the pore pattern of thecal plates and new structural details of the platelets in the periflagellar area. These morphological characteristics were compared with the closely related species within the *P. triestinum* clade, which showed synapomorphic characters in the periflagellar area (small accessory pore, platelet pattern, shape of the apical wing). Further comparison of characteristics varying between species in this clade and in the sister clade encompassing species related to *Prorocentrum micans* suggests some features of morphological evolution within this part of the genus.

1. Introduction

Prorocentrum (Ehrenberg, 1834) is a thecate dinoflagellate genus with a peculiar morphology within this lineage. The theca is composed of two large lateral plates joined by the sagittal suture, and of the periflagellar area which is a set of small platelets around the flagellar and accessory pores inserted apically between these two plates (Hoppenrath et al., 2013). The genus is distributed worldwide, mostly marine. It is diverse in terms of morphology and habitats, comprising planktonic and benthic species. For a century and half after the description of the type species *Prorocentrum micans* Ehrenberg (Ehrenberg, 1834), all species were described by light microscopy. With the advent of new technologies, first for observation by scanning electron microscopy, and then for genetic analysis mainly by rDNA sequencing, the new species were gradually described with more and more detailed and precise criteria. Thus, even for old, well-established species with worldwide distribution, it has become obvious that a new clarified description may be needed (e.g., Tillmann et al., 2019, 2022). For *P. micans* reinvestigated by Tillmann et al. (2019), this came after new cryptic species were erected (Han et al., 2016; Henrichs et al., 2013), which to some extent challenged the limits of accepted morphological plasticity in many *Prorocentrum* species (e.g., Bursa, 1959, 1962; Hulburt, 1965; Cohen-Fernandez et al., 2006). In addition, new *Prorocentrum* species are still being regularly described (e.g., Arteaga-Sogamoso et al., 2023; Tillmann et al., 2023a, 2023b; Gómez et al., 2023).

The small planktonic species *Prorocentrum venetum* Tolomio & Cavolo (length 19–21 µm, depth 13–14 µm) was first described from waters collected in Venice Lagoon (Italy), near Alberoni fort along the Canale del Lemento, during summer 1981, when the organism formed a dense and almost monospecific bloom (Tolomio and Cavolo, 1985). Original material had been stored by the authors in the cryptogamy herbarium of the Biology Department of the University of Padua (Padova, Italy), but upon request to the Biology Department, it was established that this material has been lost (L. Trainotti, pers. com.) and was therefore no longer available for further analysis. The description of *P. venetum* was one of the first made using scanning electron microscopy (SEM) for a species of *Prorocentrum*. All observations were made on formalin-fixed material: light microscopy (LM) and SEM observations (two and six

* Corresponding author.
E-mail addresses: daniel.grzebyk@umontpellier.fr (D. Grzebyk), mona.hoppenrath@senckenberg.de (M. Hoppenrath), urban.tillmann@awi.de (U. Tillmann).

https://doi.org/10.1016/j.protis.2025.126099
Received 17 September 2024; Accepted 28 March 2025
Available online 3 April 2025

published micrographs, respectively) were reported under relatively low magnifications. Cell orientation (i.e., the designation of right and left lateral thecal plates) was done following Bergh (1881) and Loeblich III et al. (1979), whereas the majority of species were described with the reverse orientation following Stein (1883), which has now become the conventional designation (Taylor, 1980; Fensome et al., 1993; Hoppenrath et al., 2013).

Since the first description of *P. venetum*, the distribution of this species has remained undocumented, as it seemed not to have been reported again in published phytoplankton records of Mediterranean waters or elsewhere (Gómez, 2008; Guiry, 2022). The validity of phytoplankton taxa never reported again after their original description can sometimes be challenged (e.g., Thessen et al., 2012). In a review examining the taxonomical status of *Prorocentrum mexicanum*, Gómez et al. (2017) proposed that *P. venetum* should be considered a synonym of *P. mexicanum*, given the similarity in cell shape and morphology of the two species. In contrast, Tillmann et al. (2022) suggested that *P. venetum* could belong to the *Prorocentrum triestinum/Prorocentrum redfieldii* lineage based on similar morphological features including the position of the periflagellar area and the pattern of thecal pores. No genetic data from specimens identified as *P. venetum* have yet been reported to date to establish the phylogenetic position of the species in the genus *Prorocentrum*. Therefore, a morphological reinvestigation of *P. venetum* and its genetic characterization with rDNA sequencing were needed.

In this paper, the isolation of two *Prorocentrum* strains from a northwestern Mediterranean coastal lagoon is reported. The general morphology, ultrastructure and rDNA phylogenetics have been investigated and LM and especially SEM morphological data were consistent with the description of *P. venetum* by Tolomio and Cavolo (1985). High magnification and resolution SEM enabled clarifying ultrastructural details of the species and the closest *Prorocentrum* species were identified by phylogenetic analysis of ribosomal DNA (rDNA).

2. Material and methods

2.1. Sampling, strain isolation and culture methods

Two *Prorocentrum venetum* strains, AYR20082019-3C4 and AYR20082019-3E9 (abbreviated AYR19-3C4 and AYR19-3E9), were isolated on 20 August 2019 from the Ayrolle Lagoon (43°04′44″N, 3°04′12″E). This shallow oligotrophic coastal Mediterranean lagoon has a surface area of 13.2 km^2 and an average depth of 0.5 m. Its water shows important annual variations in salinity and temperature (Bec et al., 2011; Grzebyk et al., 2017); on sampling day, the water temperature was 20 °C and salinity was 43. Seawater (20 litres) was filtered through a 20-µm sieve, passed onto a 5-µm sieve, and the 5–20 µm phytoplankton thus collected were then used for cell isolations. Clonal cultures were obtained by isolating a single cell by micro-pipetting using a sharpened Pasteur pipette under a Axiovert inverted microscope (Zeiss, Jena, Germany), and inoculation in a well of a 96-well culture plate containing enriched natural seawater (ENSW) culture medium (Andersen, 2005) at a salinity of 34. Cells were grown at 18.5 °C in a climate chamber with a 12:12 h light-dark photoperiod. Well-developed cultures were selected and transferred to wells of 24-well plates containing 2 ml of culture medium, and subsequently in 50-ml suspension culture flasks (Greiner Bio-One, Frickenhausen, Germany), and grown as described before.

2.2. Morphological analyses

Observation of living or fixed cells (formaldehyde: 1 % final concentration, or neutral Lugol-fixed: 1 % final concentration) was carried out using an inverted microscope (Axiovert 200 M; Zeiss, Jena, Germany) and a compound microscope (Axiovert 2; Zeiss), both equipped with epifluorescence and differential interference contrast optics. Light microscopy examination of thecal plates of cells stained with Solophenyl Flavine 7GFE500 (Chomérat et al., 2017) was performed using epifluorescence microscopy with epifluorescence filter set 09 (Zeiss; BP 450–490; FT 510; LP 515). The shape and location of the nucleus was determined after staining of formalin-fixed cells with 4′-6-diamidino-2-phenylindole (DAPI, 0.1 µg ml^{-1} final concentration) for 10 min. Images were taken either with a digital camera (Axiocam MRc5; Zeiss), or videos were recorded using a digital camera (Gryphax; Jenoptik, Jena, Germany) at full-HD resolution. Single frames were extracted using Corel Video Studio software (Version X8; Coral, Ottawa, Canada). Cell length and depth of freshly fixed cells (neutral Lugol, 1 % final concentration) from dense but healthy and growing strains during late exponential phase were measured at microscopic magnification of 1000× using the compound microscope and the Axiovision software (Zeiss).

Observations using scanning electron microscopy (SEM) were performed as described in Tillmann et al. (2023b).

For transmission electron microscopy (TEM), cells from strain AYR19-3C4 were concentrated in a microfuge tube by slow centrifugation (8 *g* for 1.5 min). The pellet was prefixed with 2.5 % glutaraldehyde in filtered seawater at 4 °C for 60 min. Cells were washed twice in filtered seawater before post-fixation with 2 % OsO_4 in filtered seawater at room temperature for 60 min. Fixed cells were dehydrated through a graded series of ethanol (30 %, 50 %, 70 %, 10 min each; 85 %, 90 %, 95 %, 2 × 100 %, 15 min each), then in 100 % propylene oxide (twice, 15 min each), infiltrated with propylene oxide-resin mixtures (2:1, 1:1, 1:2), and embedded in EMBed-812 resin (Science Services, Munich, Germany). The block was polymerized at 60 °C for 22 h and sectioned with a diamond knife on a Reichert Ultracut microtome (Reichert-Jung, Vienna, Austria). Thin sections were directly viewed under an EM 900 N TEM (Zeiss) operated at 80 kV. Digitized images were taken with a *sharp:eye* Wide-angle Dual Speed CCD-camera (TRS, Dünzelbach, Germany) operated by the ImageSP software (TRS, Dünzelbach, Germany).

Terminology of cell orientation and designation of thecal plates and platelets follows Hoppenrath et al. (2013) supplemented by Tillmann et al. (2019).

2.3. Sequencing and phylogenetic analyses

Genomic DNA (gDNA) extraction and purification was performed using the PureLink Plant Total DNA Purification kit (Invitrogen, Carlsbad, California, USA). Pelleted cells (1.0 ml of culture) were resuspended in 250 µl of provided lysis buffer R2, then after the addition of 15 µl of SDS, were incubated at 55 °C for 15 min in a in a water bath sonicator Sonorex RK100H (Bandelin, Berlin, Germany) working at 35 kHz frequency. RNAs were then digested after RNase addition and incubating again at 55 °C for 15 min in the water bath sonicator. Manufacturer's instructions were then followed, allowing gDNA adsorption onto a purification column, cleaning steps with a washing buffer, and ultimately, gDNA was eluted with 100 µl of the provided elution buffer (10 mmol l^{-1} Tris at pH 8.0). The eluted gDNA solution was supplemented with 0.2 µl of EDTA solution (0.5 mol l^{-1} at pH 8.0) and then stored at −24 °C.

An assembled rDNA sequence that included the 18S rRNA gene, the internal transcribed spacer (ITS) region (ITS1, the 5.8S rDNA, and ITS2), and the D1-D3 region of the 28S rRNA gene (hereafter called 18S–D3 sequence) was constructed with sequencing data obtained from two overlapping PCR-amplified rDNA fragments (Grzebyk et al., 2022). The PCR primers used for PCR and sequencing are described in supplementary material (Table S1). The 18S rDNA fragment was amplified with the primer pair 18S-F and 18S-PROT-R. The second rDNA fragment, which included the 18S rDNA end, the ITS region and the beginning of the 28S rDNA, was obtained with the 18S-I3F forward primer that hybridizes to the 3′ end of 18S rDNA (allowing a ~ 600-bp overlap with the 18S rDNA amplicon sequence) and the D3b-R reverse primer hydridizing at the end of D3 domain of 28S rDNA. The PCR reactions were performed using and the PrimeSTAR GXL DNA Polymerase

Kit (Takara Bio Inc., Japan) with a high-fidelity enzyme, in a Mastercycler Ep Gradient S thermal cycler (Eppendorf, Germany). The PCR programme consisted of 40 cycles: 98 °C for 15 s, 52 °C for 15 s, and 68 °C for 2 min, followed by a final elongation period at 68 °C for 2 min. The amplicons were purified with the QIAquick PCR Purification Kit (Qiagen), and sequenced with the appropriate sequencing primers (Table S1), the Big Dye Terminator V3.1 kit and an ABI 3500XL Genetic Analyzer (Applied Biosystem, Foster City, CA, USA) at the ISEM-Labex CEMEB sequencing facility (Montpellier University, France). The sequence chromatograms were checked by eye and the DNA fragments

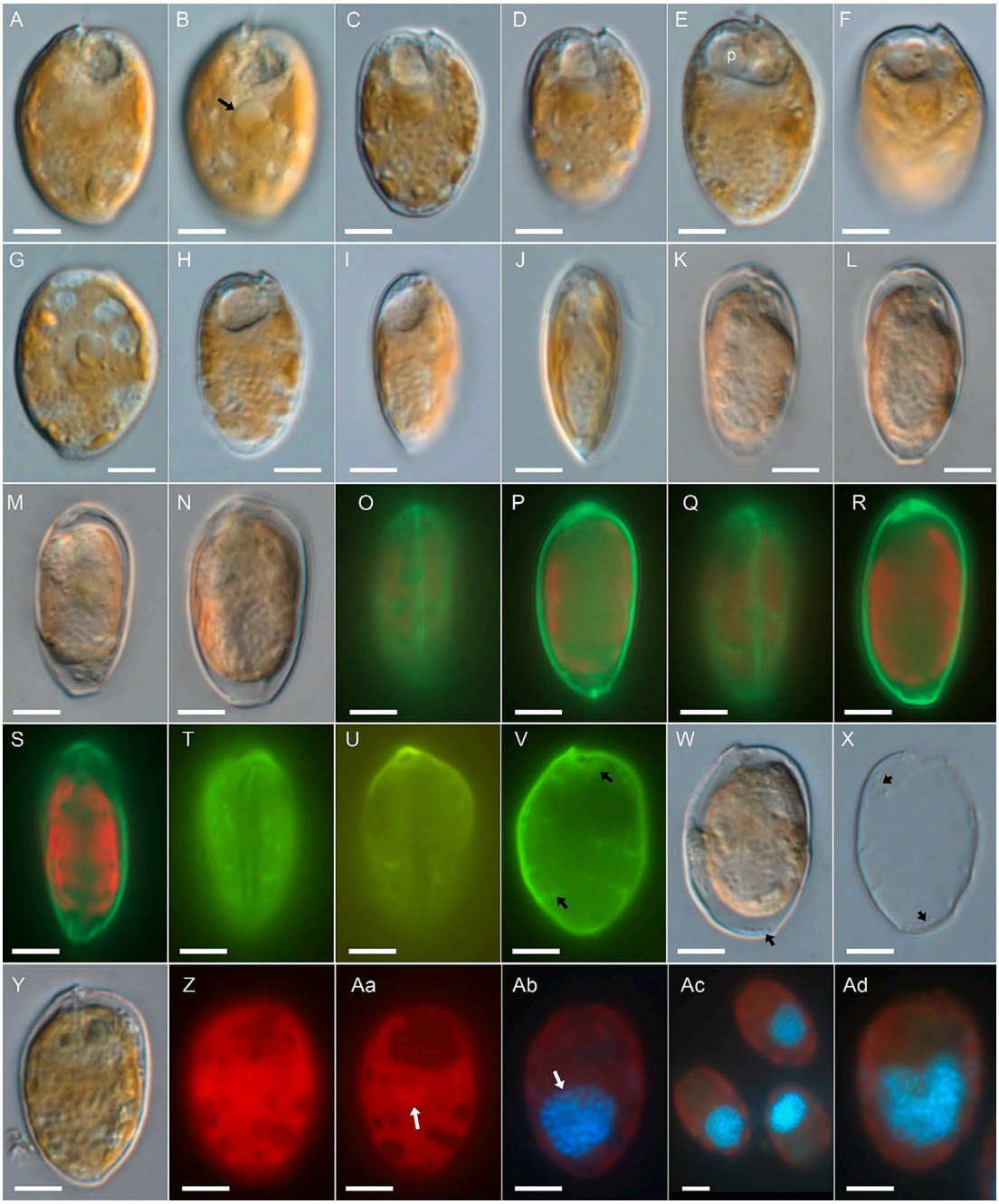

Fig. 1. *Prorocentrum venetum* (strain AYR19-3C4), LM. **A–J**. Living cells. **K–Ad**. Formaldehyde fixed cells. **A–N**. Differential interference contrast LM, general size and shape of cells in lateral view of the right thecal plate (**A, B**), the left thecal plate (**C–H**) and in ventral/dorsal view (**I–N**). Note the round to broadly oval pusule (p) labelled in **E**, and the central round pyrenoid (arrow) labelled in **B**. Also note the pointed antapical end of a presumably newly divided cell (**J**) and the truncated antapical end in broader cells (**K–N**). **O–V**. Cells stained with solophenylflavine in epifluorescence and under blue-light excitation, to illustrate plates and plate sutures (visualized by green fluorescence), and the shape and location of chloroplasts (red fluorescence), in ventral/dorsal view (**O–U**) or right lateral view (**V**). Note the lateral position of the two lobed chloroplasts (**R**, **S**) and the periflagellar area in the dorsal view (**T**) and ventral view (**U**). **V–X**. Visibility of thecal pores (arrows) when plates are stained (**V**), or when the contracted cell content allow a partial view of the plates (**W**) or on an empty theca (**X**). **Y–Ab**. The same cell stained with DAPI in brightfield (**Y**), with blue-light excitation (**Z, Aa**, two different focal planes) or with UV excitation (**Ab**), to illustrate shape and position of the chloroplasts and the nucleus (blue fluorescence). Note the central pyrenoid (arrow in **Aa**), the apical oval area void of chloroplast in **Aa**, and the antapical position of the round nucleus (arrow in **Ab**). **Ac, Ad**. DAPI stained cells with epifluorescence and UV excitation to illustrate shape and posterior position of the nucleus; the enlarged nucleus in **Ad** is presumably undergoing nuclear division. Scale bars: 5 μm. (For interpretation of the references to color in this figure legend, the reader is referred to the web version of this article.)

were assembled using the BioEdit v7.2.6.0 program (Hall, 1999).

Due to the heterogeneous distribution of reference sequence data for the genus *Prorocentrum* concerning the 18S rDNA, the ITS region and the D1-D3 region of 28S rDNA, their sequencing data were used in separate phylogenetic analyses. The 28S rDNA phylogenetic analysis focused on the D1-D2 region because the D3 domain was not determined in many reference sequences, and given the powerful phylogenetic information retained in this D1-D2 rDNA barcode region (Grzebyk et al., 2017). Reference sequences were selected by BLASTN similarity analyses (Altschul et al., 1990) using the web interface NCBI BLAST (Johnson et al., 2008) and the GenBank nucleotide database. Alignments were generated with CLUSTAL X 2.1 (Larkin et al., 2007) and were refined by eye using the BioEdit program (Hall, 1999). Phylogenetic analyses were performed with the online application Phylogeny.fr (Dereeper et al., 2008) run by the ATGC bioinformatics facility (http://www.atgc-montpellier.fr/). The "A la Carte" mode was used with the corrected alignment, in which the phylogenetic analysis pipeline implemented the maximum likelihood (ML) program PHYML 3.0 (Guindon et al., 2010) with default settings applied, including the HKY85 substitution model and four categories of substitution rates, and the estimation by the program of the Gamma distribution parameter, the proportion of invariable sites and the transition/transversion ratios. The analyses were also computed with two other substitution models: TN93 following the SMS model selection program (Lefort et al., 2017) also run on the ATGC platform, and the more complex model GTR. The estimation of branch support in the phylogenetic tree was statistically tested with the SH-like approximate likelihood-ratio test aLRT (Anisimova and Gascuel, 2006). Additional ML analyses were performed with PhyML 3.0 with one thousand bootstrap resampling for branch support estimation, with estimation of optimized equilibrium frequencies, the transition/transversion ratios, the proportion of invariable sites (I), and parameters of Gamma-shaped distribution (Γ) with 4 classes of site substitution rates. Analyses using MrBAYES (Huelsenbeck and Ronquist, 2001) were performed on the NGPhylogeny.fr bioinformatics platform (https://ngphylogeny.fr/; Lemoine et al., 2019) with the substitutions models HKY85 and GTR with one million generations, with estimation of the proportion of invariable sites and the remaining sites are Gamma-distributed (invgamma rate model); the other execution parameters were set to default (4 chains, sample frequency 500, burn-in fraction 0.25).

3. Results

3.1. Detailed description

In culture, the cells of both strains AYR19-3C4 and AYR19-3E9 were photosynthetic and had a planktonic lifestyle. Both strains shared identical morphological details. The LM and SEM morphological descriptions and all morphometric analyses were based on the study of these two strains, while the TEM ultrastructural study was carried out only with the AYR19-3C4 strain. This strain is described here (Figs. 1–6), and micrographs obtained with strain AYR19-3E9 are shown in the supplementary material (Figs. S1–S3).

Cells were 19.0–24.4 μm long, 11.4–17.4 μm deep and 8.1–15.0 μm wide; the length:depth ratio was 1.32–1.77 (Table 1). Using light microscopy, cells observed in lateral view had an oval shape with a barely visible anterior projection (Figs. 1A-H, S1A, B). The dorsal curvature was elliptic whereas the ventral curvature was more swollen and formed a ventral bulge near the anterior end, making the contour of thecal plates slightly asymmetrical. This asymmetry was accentuated by the small spine-like apical projection located in a slightly central to dorsal subapical position (Fig. 1A-E). At the posterior end, the cell shape was variable, showing nearly rounded shapes (Figs. 1C, S1C, P), or slightly pointed with rounded tip close to the vertical axis (Figs. 1V, S1O), or with a short, flattened edge with a barely visible tip slightly oriented ventrally (Figs. 1A, E, G, S1E, N, P). In dorsal/ventral view, the cell shape was lenticular (Fig. 1I-N). The posterior end was pointed in narrow cells (Figs. 1I-J, S1G, Q) but was truncate in enlarged cells (Figs. 1K-N, S1J, K, S). The pusule having the appearance of a hyaline sack structure was located in the anterior part of the cell (Figs. 1A-F, H, I, S1B-E). Golden-brown coloration in light microscopy and red fluorescence of chlorophyll under the epifluorescence microscope showed two lobed chloroplasts extending laterally under each thecal plate (Figs. 1A-J, P-S, Z, S1B-E, O–U, W), often having an indentation occupied by the pusule system in the anterior end of cell (Fig. 1 Aa). In lateral view, a putative roundish pyrenoid was sometimes visible in central position of cells, between the pusule and the nucleus (Fig. 1B, D, F, G, Aa). The round nucleus occupied most of the posterior half of the cell (Figs. 1C, E, G-L, Ab-Ad, S1C, H–N, X). The nucleus shape could be more irregular probably in early stage of nuclear division (Fig. 1 Ad). Thecal pores were difficult to recognize and visible only without cellular content (Fig. 1W, X) or after theca staining (Fig. 1T-V). Rod-shaped structures (trichocysts) were not observed in the anterior cell area.

Scanning electron microscopy observations were obtained from both strains (strain AYR-3C4: Figs. 2–3; strain AYR-3E9: Figs. S2-S3). Morphometric data showed moderate variations in the morphological features of the cells within and between the two strains (Table 1). The thecal surface of the two plates and the periflagellar platelets was smooth (Figs. 2, 3, S2, S3). The intercalary band at the suture of thecal plates was almost lacking in narrow cells (Figs. 2A, E-F, S2C), and was broad and smooth with transverse striations in large cells (Figs. 2C, I, L, S2G–I). Both lateral plates were perforated with pores except in their central area (Figs. 2A-I, S2A-G). There were three different types of pores (Figs. 2K-N, 3F-J, S2M). The first two, denoted as large and small pores, were each in similar numbers on the right and left plates (Table 1; Fig. 4A, B). The large pores were numerous (24–39 per thecal plate) and consisted of a circular depression (0.31–0.61 μm outside diameter) at the bottom of which was a small round orifice (0.11–0.22 μm in diameter) at the top of a tubular structure (Fig. 3F, I, J). The internal tubular structure could be oblique (Fig. 3G, H). There were fewer small pores (7–17 per plate) which were flush with the plate surface and were generally scattered near the large pores (Figs. 3F-J, 4A-E). The mean diameter of the pore orifice of small pores (0.11–0.16 μm) was similar to that of large pores (Table 1), but the orifice diameter of large pores was more variable (up to 0.22 μm, Table 1). The third type of pore (denominated as mini-pore) was a tiny, single pore located at the slightly protruding tip at the posterior end of the cell (Figs. 3I, J, S2M). Its diameter < 0.1 μm was significantly smaller than the orifice of the other pores. The mini-pore was difficult to identify or was not always observed on examined plates.

On the two lateral plates, large and small pores were arranged together in groups, whose positions were approximately mirror-arranged on the right and the left plates (Fig. 4A-B, E). Groups were numbered clockwise on the right plate starting from the ventral edge of the periflagellar area and ending at the dorsal edge (from R1 to R10) (Fig. 4 Ei), and symmetrically counter-clockwise on the left plate (L1 to L10) (Fig. 4 Eii). In each group, the number of pores varied by a few units between cells of each strain and between the two strains (Supplementary Tables S2, S3), and the location of each pore varied more or less on the plate and in relation to neighbouring pores. Most groups contained a single small pore, but there were often two in R2/L2 and R9/L9 (Fig. 4E). Only R6/L6 did not have a small pore but sometimes a mini-pore instead. In pore groups, pores were either scattered or arranged in short rows (Figs. 2A-I, 4A, B). On the right plate, the first row of pores R1 was located on the ventral edge of the periflagellar area along platelets 4 and 5 (Figs. 2K, L, 3A, B, 4Ei), while pores in the homologous row L1 were aligned approximately perpendicular to the edge of plate (Figs. 2D, E, N, 4Eii). The anterior half of plates had three other groups with scattered pores, one on the ventral edge (R2/L2) and two on the dorsal edge (R9/L9 and R10/L10) (Figs. 2A-I, 4E). On the posterior half, the smallest group of pores (R5/L5) contained only one large and one small pore (Figs. 3F, I, J, 4E) and there were five rows of pores (Figs. 2A-I, 4E).

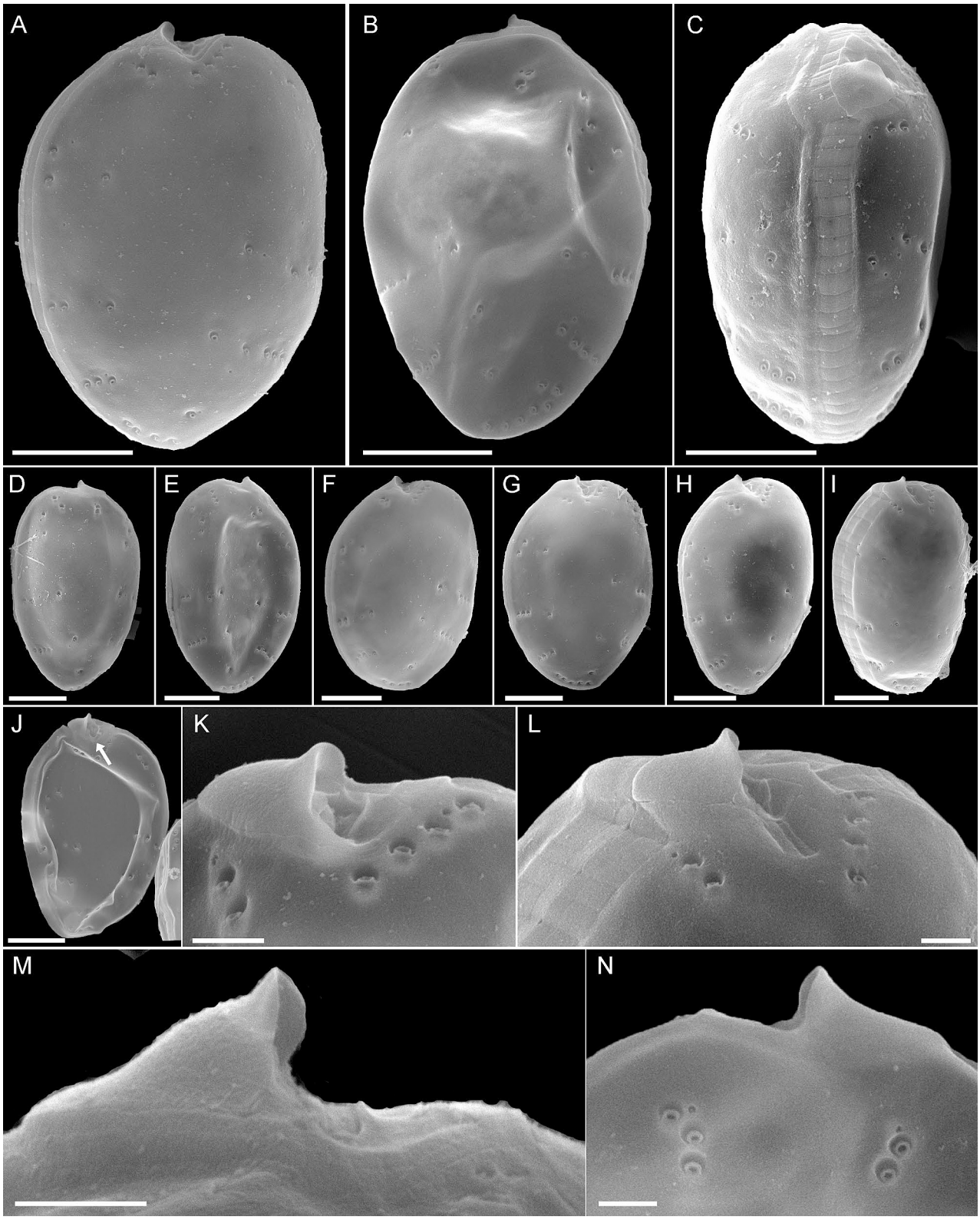

Fig. 2. *Prorocentrum venetum* (strain AYR19-3C4), SEM. **A–I**. Entire cells in right thecal view (**A, F–I**), in left thecal view (**B, D, E**), or in dorsal apical view (**C**, an enlarged cell with a broad, transversely striated, intercalary band). **J**. Flattened right thecal plate showing the apical V-shaped insertion of the periflagellar area (arrow). **K–N**. Detail views of the apical area in right apical view (**K**), right dorsal view (**L**), in right lateral view (**M**) and in left lateral view (**N**). Scale bars: 5 μm (**A–J**) or 1 μm (**K–N**).

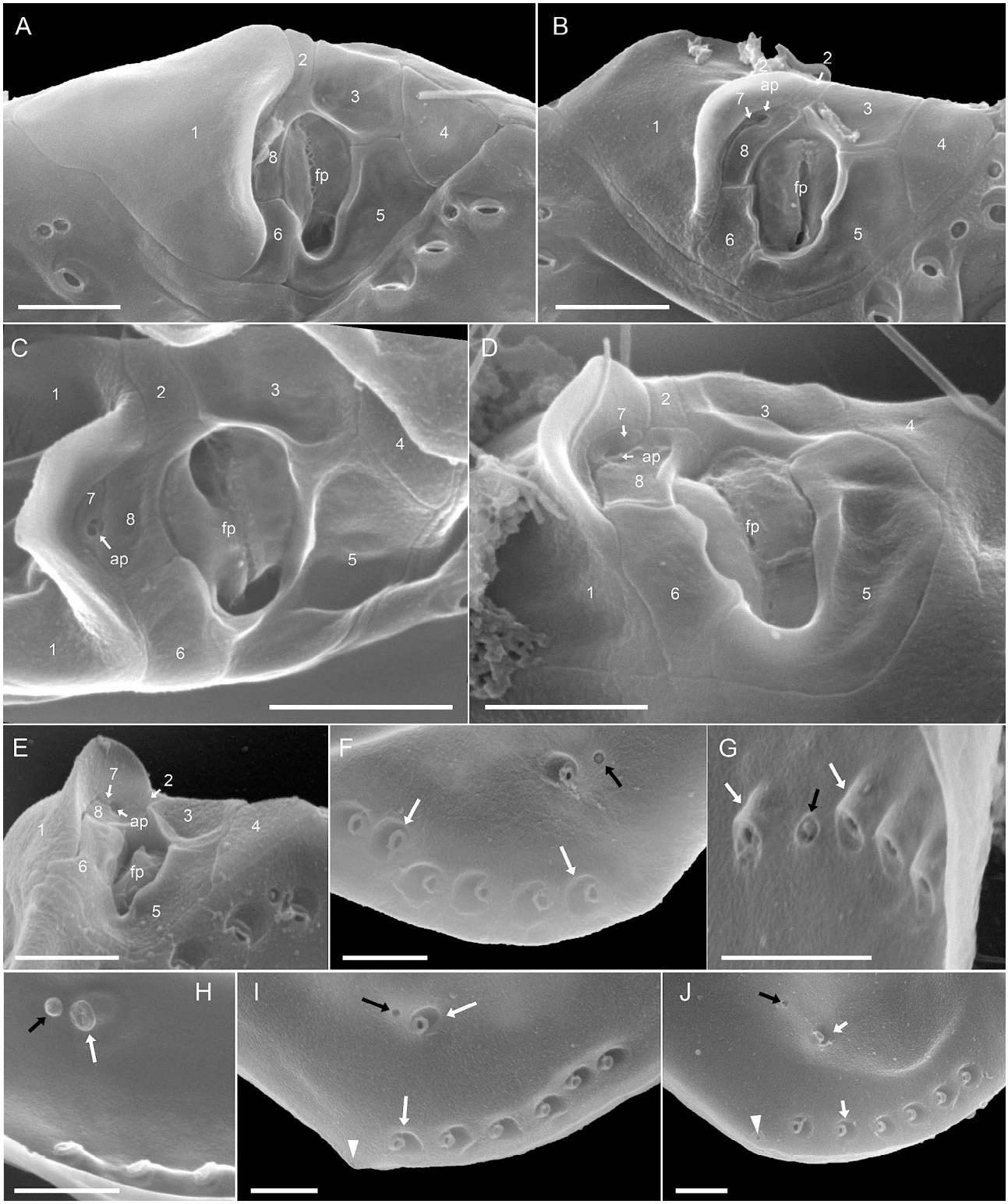

Fig. 3. *Prorocentrum venetum* (strain AYR19-3C4), detailed SEM of the periflagellar area, surface structure and pores. **A–E.** The periflagellar area in apical view (**A–C**), right lateral view (**D**) or apical ventral view (**E**). **F–J.** General appearance of thecal pores (large pores: white arrows; small pores: black arrows) in external view (**F, I, J**) or in internal view showing the internal tubular shape of large pores (**G, H**). At the posterior end of cells (**I–J**), note the presence of a mini-pore (white arrowhead) located at the slightly protruding tip of the thecal plate, the diameter of which is distinctly smaller than that of the small pores (black arrows). Platelet numbering according to Hoppenrath et al. (2013); ap = accessory pore, fp = flagellar pore. Scale bars: 1 μm.

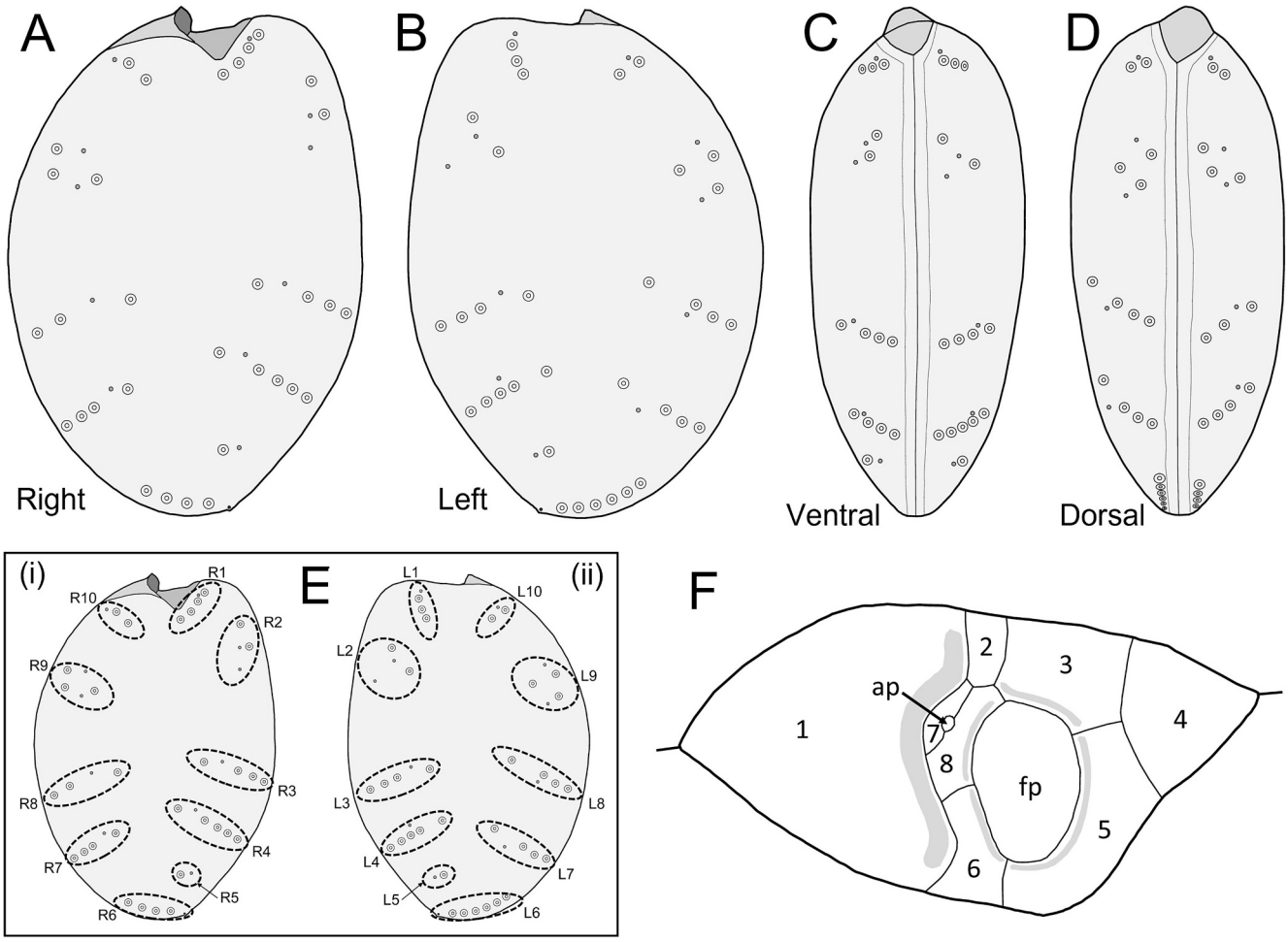

Fig. 4. Schematic drawings of *P. venetum*. The numbers of pores (large and small) are representative of the mean/median numbers for strain AYR19-3C4 (Table 1, Tables S2 and S3). **A.** Right lateral view. **B.** Left lateral view. **C.** Ventral view. **D.** Dorsal view. **E.** Labeling of pore groups on **(i)** the right lateral plate (R1 to R10 groups) and **(ii)** the left lateral plate (L1 to L10 groups). **F.** Periflagellar area in apical view (the gray surfaces correspond to the base of the erect structures above the platelets). Platelet numbering according to Hoppenrath et al. (2013); ap = accessory pore, fp = flagellar pore.

Four rows radiated almost perpendicularly from the plate edge: two rows from the ventral curvature (R3/L3 and R4/L4) and two from the dorsal curvature (R7/L7 and R8/L8). In the last row (R6/L6), the large pores were arranged evenly spaced along the dorsal edge of the posterior end (Figs. 3F, I, J, 4A, B, D).

The periflagellar area was enclosed in a shallow V- to U-shaped recess in the right thecal plate, much of it located ventrally to the longitudinal axis of the cell (Figs. 2A, F, G, 4A, S2A, E, F). It was approximately lenticular in shape (Figs. 3A, B, 4F), with dimensions of 3.4–4.3 µm in depth and 1.7–2.5 µm in width (Table 1). It was composed of eight platelets: 1, 2, 3, 4, 5, 6, 7, 8 (Figs. 3A-E, 4F, S3). The dorsally located platelet 1 was the largest, with a size making nearly half of the periflagellar area. It was roughly triangular in shape and partly elevated (forming a sort of hump) above to the edge of the lateral plates (Figs. 2K, M, N, 4F). Platelet 1 bore the most prominent apical projection (0.80–1.43 µm high; Table 1), rising on the internal edge along platelets 2, 7, 8 and 6 (Figs. 3A-D, 4F). This very broad projection was a wing with a visor shape, rising above platelet 7 and the accessory pore (Figs. 2K, 3A, 4F, S3). The ventral platelet 4 was flat (Figs. 3A-E, S3). The flagellar pore was surrounded by platelets 3, 5, 6 and 8, all of which bore a low list bordering the pore as a sort of collar (Figs. 3A-E, 4F). The list on platelet 6 pointed in the form of a small protrusion rising slightly above the pore (Figs. 3B, D, E, S3). The flagellar pore was oval in shape, measuring 0.9–1.3 µm long and 0.6–0.9 µm wide (Table 1); it was closed by two lip-like structures (Figs. 3A-B, S3). The accessory pore was inserted between platelets 7 and 8; it was approximately round and tiny in size with a diameter of ~0.15 µm (Figs. 3B-D, 4F, S3).

Intracellular ultrastructure examined by TEM (Figs. 5, 6) complemented observations made by light and epifluorescence microscopy. The large dinokaryotic nucleus in the posterior half of the cell contained the typical condensed chromosomes and a nucleolus (Fig. 5A, B, D). Mitochondria with tubular cristae and oil droplets were distributed in the cytoplasm (Fig. 5A, B), and the Golgi apparatus was observed (Fig. 5F). The membrane system of the pusule was visible below the flagellar pore region (Fig. 5C). Trichocyst cross sections of different diameter were spread in the cell (Fig. 5B, E). Chloroplast parts (lobes) were located in the cell periphery directly below the thecal plates (Fig. 5A, B). The pyrenoid can be of an irregular interlamellar type (immersed, internal; Fig. 6A, B) or more often of a bulging (terminal) type without starch sheath (Fig. 6 C–F). Single thylakoids or stacks of two traversed the pyrenoid matrix in no ordered manner (Fig. 6).

3.2. Molecular phylogenetics

The size of the rDNA sequence of *P. venetum* strain AYR19-3C4 (accession number PP258975) – comprising the 18S rDNA, the ITS region and the D1-D3 region of the 28S rDNA – was 3326 base pairs (bp) between the two external PCR primer-binding sites (abbreviated as 18S–D3), which was the same length as for the *P. redfieldii* strain CCMP1919 (accession number ON491170). The obtained sequence from

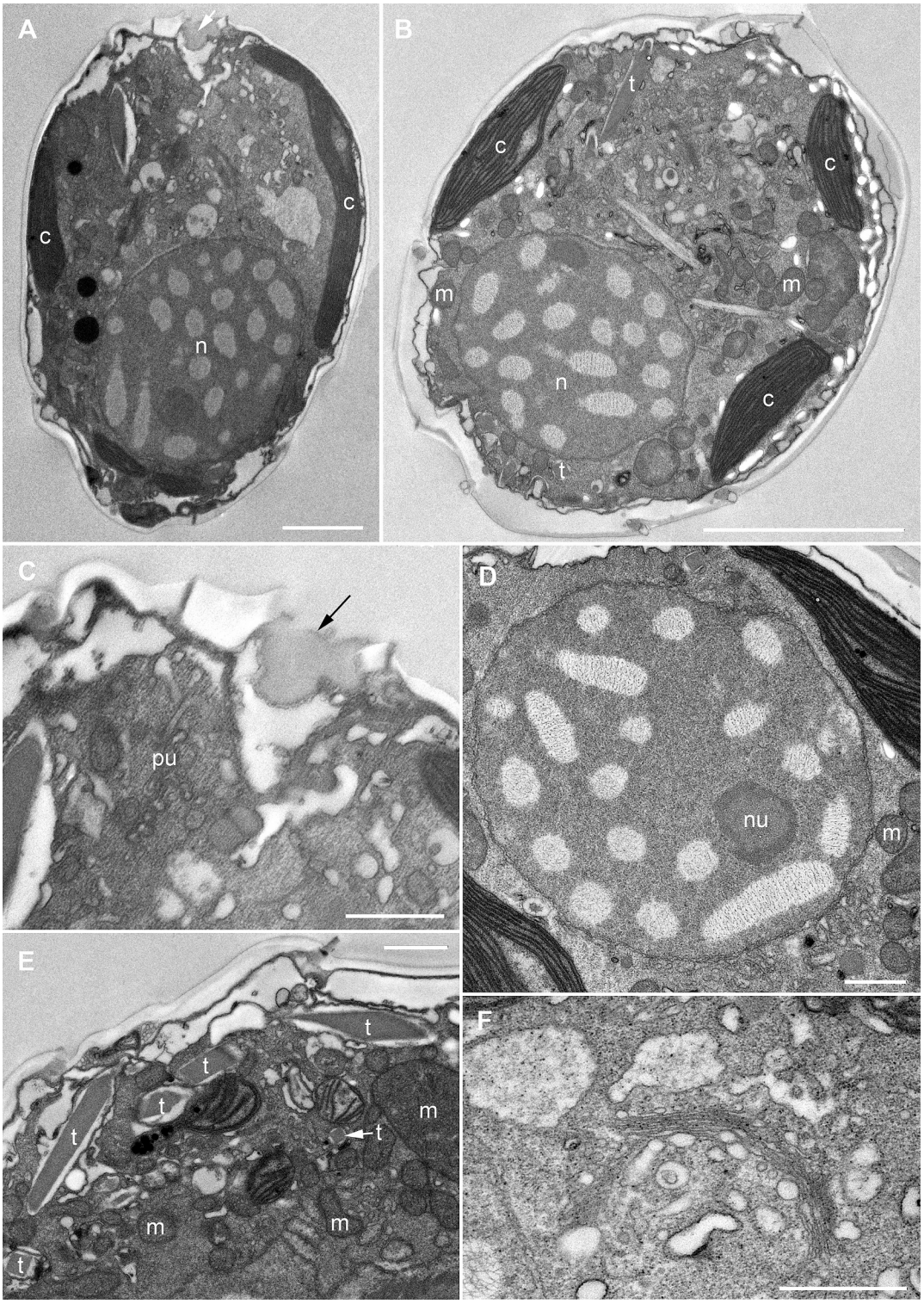

Fig. 5. *Prorocentrum venetum* (strain AYR19-3C4), transmission electron microscopy of the general cell ultrastructure. **A.** Longitudinal section showing part of the anterior periflagellar area with flagellar pore (white arrow) and the posterior nucleus (n), peripherally arranged chloroplast parts (c) and dense black oil droplets. **B.** Oblique section showing the nucleus (n), chloroplast lobes (c), mitochondria (m) and trichocysts (t). **C.** Anterior cell region below the periflagellar area (black arrow pointing into the flagellar pore region) with membranes of the pusule system (pu). **D.** Nucleus with condensed chromosomes and nucleolus (nu). **E.** Cross sections of trichocysts (t) of different diameter and an oblique longitudinal section. **F.** Part of the Golgi apparatus. Scale bars: 2.5 µm (**A**), 5 µm (**B**), 1 µm (**C**–**F**).

strain AYR19-3E9 (from end of 18S to the end of D3 region of the 28S rDNA, accession number PP258976) was identical to those from strain AYR19-3C4. Verification of sequencing chromatograms did not show any clear evidence of single nucleotide polymorphisms shared in the two *P. venetum* strains.

Phylogenetic analysis of the genus *Prorocentrum* based on 18S–D3 sequences (Fig. 7, Supplementary Figs. S4-S5) showed that *P. venetum* belonged to a well-supported clade formed with *P. triestinum* and *P. redfieldii*. This triadic clade was sister to a clade containing the species *P. micans*, *P. koreanum*, *P. texanum*, *P. rhathymum* and *P. steidingerae*.

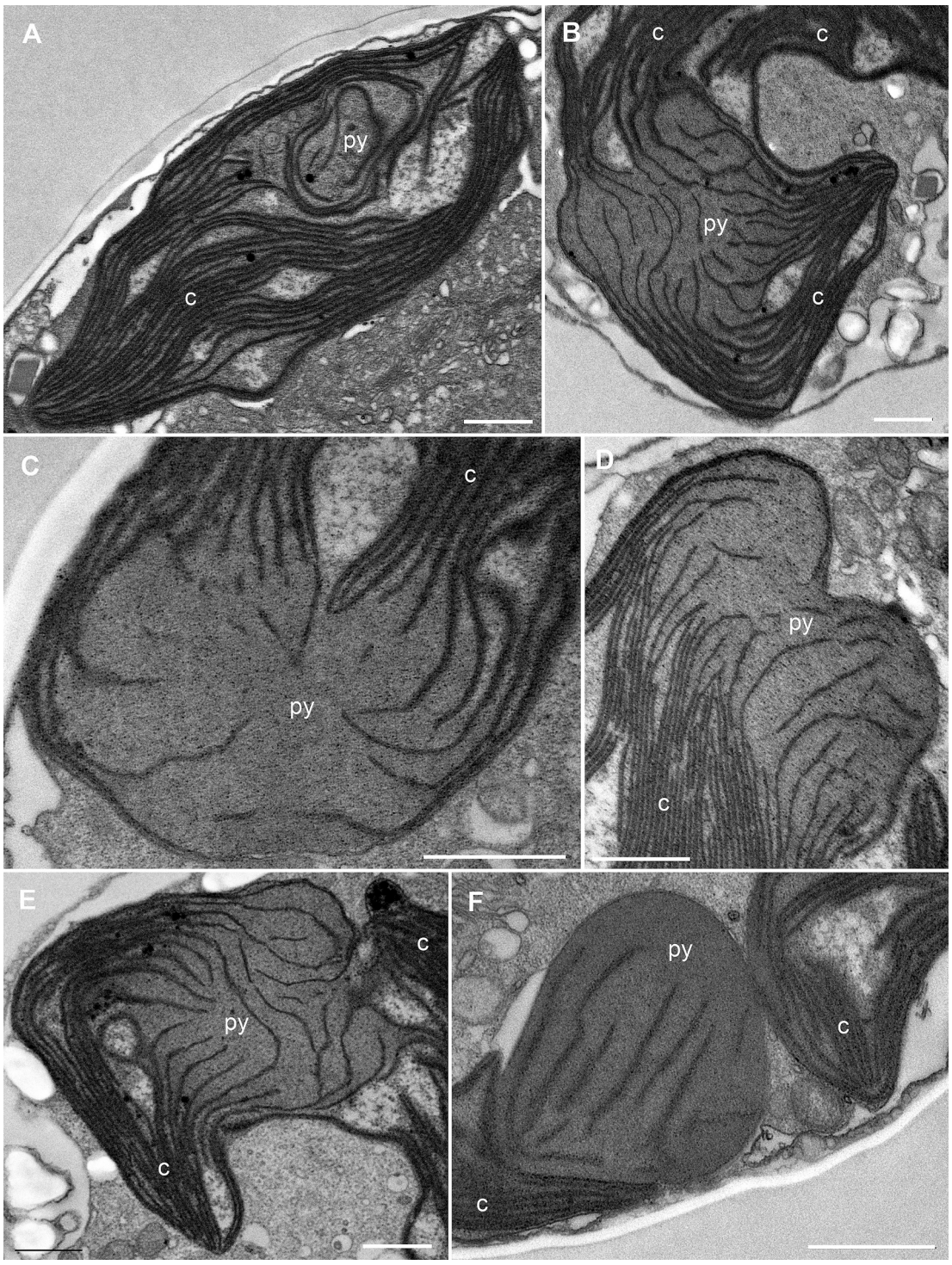

Fig. 6. *Prorocentrum venetum* (strain AYR19-3C4), transmission electron microscopy of chloroplast (c) details. **A**, **B**. Irregular interlamellar pyrenoid (py). **C**–**F**. Different morphologies of the bulge-type pyrenoid (py) without starch sheath. Note the thylakoids, single or bundled in pairs, which cross the pyrenoid matrix in an unordered manner. Scale bars: 1 μm.

Accordingly, the subsequent phylogenetic analyses were conducted with selected sequences belonging to these two sister clades (Supplementary Figs. S6-S8, see below). The alignment of nucleotide sequences from *P. venetum*, *P. triestinum* and *P. redfieldii*, showed an identical pattern with many shared gap positions and specific substitutions in this clade with respect to sequences from other *Prorocentrum* species (Supplementary Fig. S9). Between the three species, some shared substitutions alternated two by two (Supplementary Fig. S9). The nucleotide sequences of *P. venetum* and *P. triestinum* showed fewer nucleotide substitutions between them as compared to *P. redfieldii* (Table 2).

In the phylogenetic trees obtained with selected nucleotide sequences of the three rDNA regions (18S, D1-D2 region of 28S, and ITS region) (Supplementary Figs. S6-S8), species relationships were not resolved unequivocally within the triadic clade between *P. venetum*, *P. triestinum* and *P. redfieldii*, as well as within the sister clade encompassing species related to *P. micans*. In the 18S rDNA analysis

Table 1
Morphometric measurements for the two strains of *Prorocentrum venetum*. The dimension values are in µm. For each strain, the provided values for the morphological features are: average (in bold) and standard deviation, the range of variation of the observations and the number (n) of observations.

Cell features		Strain	
		AYR19-3C4	AYR19-3E9
Cell dimensions	Length (l)	**21.5** ± 1.0 19.5–24.4; *n* = 78	**21.9** ± 1.0 19.0–24.4; *n* = 63
	Depth (d)	**14.1** ± 1.0 11.7–16.3; n = 63	**14.6** ± 1.2 11.4–17.4; *n* = 43
	Width (w)	**11.0** ± 1.8 8.1–15.0; *n* = 15	**11.7** ± 1.5 8.3–14.9; *n* = 20
Dimension ratios	length:depth	**1.52** ± 0.1 1.33–1.77; n = 63	**1.52** ± 0.1 1.32–1.77; n = 43
	length:width	**1.94** ± 0.3 1.57–2.52; n = 15	**1.88** ± 0.2 1.52–2.49; n = 20
Platelet-1 wing	Height	**1.11** ± 0.1 0.80–1.43; *n* = 28	**1.10** ± 0.2 0.80–1.40; *n* = 18
Diameter of lateral plate pores	Large pore outer diameter	**0.43** ± 0.06 0.31–0.56; *n* = 27	**0.42** ± 0.07 0.32–0.61; n = 20
	Large pore inner diameter	**0.15** ± 0.02 0.11–0.22; n = 27	**0.14** ± 0.03 0.11–0.22; n = 20
	Small pore diameter	**0.13** ± 0.01 0.11–0.16; n = 20	**0.13** ± 0.01 0.12–0.16; n = 20
Number of pores per lateral plate	Right plate large pores	**32.1** ± 4.1 25–38; *n* = 38	**32.4** ± 4.1 24–39; n = 18
	Right plate small pores	**11.5** ± 1.8 7–16; *n* = 39	**9.8** ± 1.7 7–13; n = 18
	Left plate large pores	**33.7** ± 3.5 25–39; *n* = 17	**31.7** ± 2.7 28–36; *n* = 9
	Left plate small pores	**11.4** ± 2.5 8–17; n = 17	**9.4** ± 1.9 7–13; n = 9
Periflagellar area dimensions	Depth	**3.9** ± 0.2 3.6–4.2; n = 9	**3.7** ± 0.3 3.4–4.3; n = 6
	Width	**2.1** ± 0.2 1.8–2.5; n = 9	**2.0** ± 0.1 1.7–2.2; n = 6
Flagellar pore	Length	**1.1** ± 0.1 0.9–1.3; n = 9	**1.1** ± 0.1 1.0–1.3; n = 6
	Width	**0.7** ± 0.1 0.7–0.9; n = 9	**0.7** ± 0.1 0.6–0.8; n = 6

(Supplementary Fig. S6), the range of genetic variations within the clade between the three species (within which the *P. redfieldii* strains exhibited genetic heterogeneity) was similar to that inside the large clade encompassing *P. micans* with five other documented species (*P. gracile*, *P. texanum*, *P. koreanum*, *P. rhathymum* and *P. steidingerae*). The analyses based on D1-D2 region of 28S rDNA (Supplementary Fig. S7) and the ITS hypervariable region (Supplementary Fig. S8) showed slightly greater genetic difference between *P. venetum* and *P. triestinum* and the species clade of *P. redfieldii*. In both of these rDNA regions, unlike the 18S rDNA, the range of genetic variation between species clades was much smaller in the *P. triestinum* clade than in the sister clade encompassing *P. micans*.

4. Discussion

From the examination of the oval cell shape, the size of cells, the distribution pattern of large thecal pores, the location and shape of the periflagellar area, and the visor shape of the apical wing (spine-like in LM), the morphological observations presented herein were consistent with the description of specimens of *P. venetum* by Tolomio and Cavolo (1985). Thus, both strains (AYR19-3C4 and AYR19-3C9) could be unambiguously identified to species level. Therefore, the first genetic fingerprint of *P. venetum* can be provided in the present study, even when the reinvestigated strains were not collected from the type locality of Venice (Italy) but from another Mediterranean lagoon environment. There is no certainty as to why the species *P. venetum* has apparently not been recorded since its description: is it because of its small size, its ordinary oval shape without distinctive signs under the LM, or its description that went unnoticed or forgotten? For example, in the long-term environmental monitoring study carried out in the Venice Lagoon, including phytoplankton sampling, blooms of *P. triestinum* and *P. rhathymum* were reported (although without any documentation on the identity of the species), but not of *P. venetum* (Bernardi Aubry et al., 2021).

A comparison of morphological details of physical type material was not possible (see Introduction). Overall, the size and oval shape of the cell contour when viewed laterally, asymmetrical at the anterior and posterior ends relative to the long axis of the cell, matched the description by Tolomio and Cavolo (1985). Generally, the shape of the posterior end of the cells varied slightly and was not well rounded (Figs. 1A, E, G, 2G-I). Although Tolomio and Cavolo (1985) did not explicitly mention such variability and deviation from the oval contour, this can be seen by carefully examining the two light micrographs (Figs. 1 and 2) provided by these authors. The strains of *P. venetum* showed a wider range in the number of large pores per plate (24–39), overlapping the range (35–40) reported in the original description. In their original description, Tolomio and Cavolo (1985) did not mention the presence of different types of pores (in particular, no differentiation of small pores), but this could be explained by the lower magnification and resolution applied in their SEM study: the small pores and especially the mini-pore at the posterior end could simply have been overlooked.

The phylogenetic analysis showed that *P. venetum*, *P. triestinum* and *P. redfieldii* formed a well-supported clade. *P. venetum* and *P. triestinum* were closer to each other with fewer nucleotide substitutions between them, while *P. redfieldii* appeared more distant and more recently derived (Table 2). The analysis also strongly supported the sistership of the *P. triestinum* clade and a large clade encompassing species related to *P. micans*.

Morphologically, *P. venetum* shares similarities with *P. triestinum* with regard to the cell size and the subapical position of the periflagellar area, but the thecal plates of *P. triestinum* are more strongly

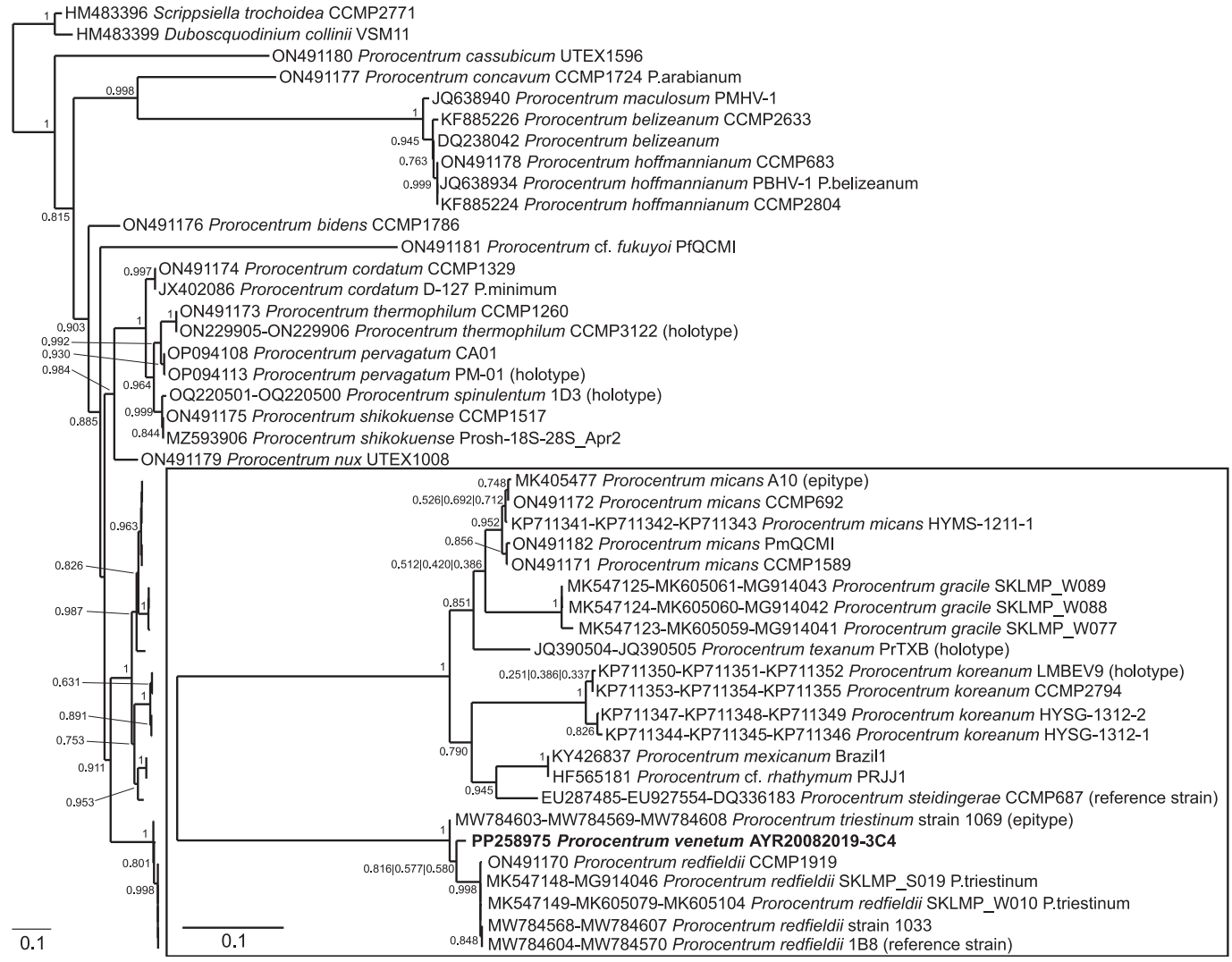

Fig. 7. Phylogenetic tree of *Prorocentrum* genus showing the position of *P. venetum* (this study, in bold), based on 18S–D3 rDNA sequences; two taxa belonging to the order Peridiniales were used as outgroups. In the box, a subtree with the same topology focusing on the two sister clades (containing taxa related to *P. micans* and *P. venetum*, respectively) is provided to better show the genetic distances between and within species clades. The tree construction was performed by the maximum likelihood algorithm with the substitution models HKY85, TN93 and GTR, which yielded identical topologies. Branch support was assessed by the aLRT method; for clarity, the value obtained with the analysis with the HKY85 model (often the highest of the three models) is shown at the main nodes, and only values that differ by more than ±0.050 are indicated as HKY85|TN93|GTR. The branch length is proportional to the number of substitutions per site (the scale bar represents the number of nucleotide substitutions per site).

asymmetrical, are lanceolate with an acute posterior end, and the periflagellar area is positioned dorsal to the longitudinal axis (Tillmann et al., 2022). Other features identified as being shared between *P. venetum*, *P. triestinum* and *P. redfieldii* are in the thecal pore pattern and the arrangement of the periflagellar area (see below). Furthermore, regarding intracellular ultrastructure, *P. venetum* has the same type of pyrenoid as *P. redfieldii* (Ndhlovu et al., 2017). In *P. micans* and *P. texanum*, the ultrastructure of the pyrenoid is different (Kowallik, 1969; Henrichs et al., 2013): it is a compound interlamellar pyrenoid that is crossed by parallel thylakoid lamellae in a regular and organized manner; this part of the chloroplast can be swollen and then projects into the cell (Dodge and Crawford, 1971).

The three types of thecal pores seen in *P. venetum* are similar in size and shape to those present in *P. triestinum* and *P. redfieldii* (Tillmann et al., 2022). The three types of pores were also described in *P. micans* (Tillmann et al., 2019), and were likely observed in other species where small pores were described with a large variability in their diameter, including *P. texanum* (range 0.08–0.13 µm; Henrichs et al., 2013), *P. elegans* (range 0.09–0.16 µm; David et al., 2014), and as observed in *Prorocentrum caribbaeum* (Faust, 1993, in Fig. 22).

Regarding the arrangement of large pores (trichocyst pores) on the thecal plates, *P. venetum* has the highest number of pores in the *P. triestinum* clade, about twice as many as in the two other species and the same is observed for small pores. All three species have a similar row of pores at the posterior end along the dorsal edge of the thecal plates (i.e., corresponding to pore groups R6/L6 of *P. venetum*), a configuration not observed elsewhere in the genus. In contrast, *P. venetum* is the only species of its clade with two pairs of radial rows of pores (with ≥3 large pores) on the dorsal and ventral edges of plates, although some pores are present in similar locations in the pore patterns of *P. triestinum* and *P. redfieldii*.

The periflagellar areas are very similar and have an identical eight-platelet pattern between *P. venetum*, *P. triestinum* and *P. redfieldii* (Tillmann et al., 2022). The most specific common feature of this *P. triestinum* clade is that the accessory pore is very small in size and is therefore hardly visible in the middle of junction between the very small platelet 7 and the platelet 8. In contrast, in species of the sister clade encompassing *P. micans*, the large accessory pore has a lenticular shape

Table 2
Numbers of nucleotide substitutions in the three considered rDNA regions for phylogenetic analyses between species two by two, between *P. venetum* (strain AYR20082019-3C4, from one continuous sequence: PP258975), *P. triestinum* (strain 1069, from three discontinuous partial sequences: MW784603, MW784569 and MW784608) and *P. redfieldii* (strain CCMP1919, from one continuous sequence: ON491170). The length of the three available rDNA fragments used for comparison for representative strains of the three species are given in the diagonal boxes (written in bold).

	P. venetum	*P. triestinum*	*P. redfieldii*
P. venetum (strain AYR-3C4)	**18S: 1748 bp** **ITS: 584 bp** **28S D1-D2: 676 pb**	18S (1593 bp): 2 ITS (524 bp): 3 28S D1-D2 (557 bp): 2	18S (1748 bp): 3 ITS (584 bp): 6 28S D1-D2 (676 pb): 5
P. triestinum (strain 1069)		**18S: 1593 bp** **ITS: 524 bp** **28S D1-D2: 557 bp**	18S (1593 bp): 5 ITS (524 bp): 7 28S D1-D2 (557 bp): 3
P. redfieldii (strain CCMP1919)			**18S: 1748 bp** **ITS: 584 bp** **28S D1-D2: 676 pb**

whose long axis is parallel to the junction between platelets 7 and 8 (Hoppenrath et al., 2013; Tillmann et al., 2019). In addition, in the *P. triestinum* clade, platelets 7 and 8 are significantly smaller and differently shaped compared to the *P. micans* clade, and the platelet 1 is relatively larger in size while platelets 2 and 6 have a reduced size. Additionally, in the *P. triestinum* clade, the apical projection rises from an almost linear base along the inner edge of platelet 1, between the right and left thecal plates, which configuration is also present in various other *Prorocentrum* species (Hoppenrath et al., 2013). In contrast, in the *P. micans* clade, the base of the spine first rises along the right inner edge of platelet 1 then turns toward the outer dorsal end of platelet 1 following the edge of the left plate, giving the spine its characteristic curved shape (named "long spine with sail" in *P. micans*, Tillmann et al., 2019), as it is clearly observable in *P. texanum* (Henrichs et al., 2013) and *P. koreanum* (Han et al., 2016), *P. gracile* (Pei et al., 2022), *P. caribbaeum* (Faust, 1993), *P. gibbosum* (Tolomio, 1988) and *P. arcuatum* (Skejić et al., 2017), and with the wing of *P. rhathymum* (Loeblich et al., 1979; Lim et al., 2013) and *P. steidingerae* (Figs. 5–10 in Faust, 1990, after Gómez et al., 2017). On the ventral side of the peri-flagellar area, the platelet 4 is flat in the *P. triestinum* clade whereas it is flanged with a short wing along its inner edge (next to platelets 3 and 5) in the *P. micans* clade.

As already discussed by Tolomio and Cavolo (1985), *P. venetum* presents similarities in shape and size with *P. brochii* J.Schiller which was described by Schiller (1918) in Adriatic waters, but this species has a more pointed posterior end, although the cell shape of *P. venetum* conforms better to another drawing of *P. brochii* published by Schiller in 1928 (pl. 3, Fig. 3). However, *P. brochii* is clearly different to *P. venetum* by the presence of (very) large pores scattered over the thecal plate as shown in the drawing reproduced in Schiller (1918, 1928, 1933) and sometimes having thick plates. Schiller (1933, pp. 41-42) synonymized *P. brochii* with *Prorocentrum maximum* (Gourret) J.Schiller, (basionym *Postprorocentrum maximum* Gourret), although the latter (whose size was not precisely given) had a very different cell shape (Gourret, 1883; Schiller, 1933, p. 41, fig. 44c). Overall, it is possible that *P. brochii* as described by Schiller (1918, 1928) is closely related to *P. venetum* and *P. triestinum* (Schiller, 1918; Tillmann et al., 2022), but detailed morphological and molecular studies on strains from the type locality of *P. brochii* are needed.

Prorocentrum ovale (Gourret) Schiller was described by Gourret (1883) with *P. maximum* in the coastal waters of the Bay of Marseille (France, northwestern Mediterranean), nearly 190 km east of the Ayrolle lagoon from where the present strains of *P. venetum* were isolated. The overall oval shape of *P. venetum* is different from *P. ovale* (Gourret, 1883), which has a much more prominent anterior ventral bulge. The length:depth ratio is greater in *P. ovale* than in *P. venetum* (~2.0 versus ~1.5, respectively). *P. ovale* has a thin, long apical spine that was described by Gourret (1883) as resembling that of *P. micans*: this spine points straight forward and clearly extends beyond the ventral bulge (by almost half its length). The size of *P. ovale* was not precisely stated, but Gourret (1883) compared and related this species to *P. micans*, suggesting that their sizes were similar.

Compared to *P. venetum*, *P. mexicanum* (Osorio Tafall, 1942) is larger (39 μm long, 29 μm in depth). The drawing of a cell in right lateral view shows that the ventral bulge is less prominent; moreover, the dorsal and ventral curvatures are almost elliptical and symmetrical with respect to the transverse axis of lateral plates whereas the ventral curvature is asymmetrical in *P. venetum*. On the surface of the thecal plate, the drawing shows scattered large pores (described by the Spanish term "puntuaciones") and a series of striations (described as tiny spines). The apical spine of *P. mexicanum* is also different from the winged projection of *P. venetum*: it points straight forward and is longer with a length about one tenth of the length of the cell. The author indicated that it was thin and slightly curved, and with a delicate "wing" visible in dorsal/ventral view.

Comparing *P. venetum* to *Prorocentrum rhathymum* (Loeblich III et al., 1979), in relation to their oval shape, Tolomio and Cavolo (1985) highlighted several differences including the dimensions (larger in *P. rhathymum*, with the length of cell in the range 32–39 μm), the shape without prominent ventral bulge, the distribution of more numerous trichocyst (large) pores in *P. rhathymum* (but not indicating precisely what differences), and the structure of the anterior spine (as described above). Indeed, *P. rhathymum* is notably distinguished by having four pairs of radial rows of pores and the absence of the dorsal row of pores on the two lateral plates.

Comparison of morphological characteristics and rDNA phylogenetical analyses has been used to discuss evolution within the genus *Prorocentrum* (e.g., Grzebyk et al., 1998; Murray et al., 2007, 2009; Boopathi et al., 2015; Zhang et al., 2015; Chomérat et al., 2019). Based on nuclear rDNA or mitochondrial genes, analyses revealed the existence of various clades within the genus *Prorocentrum*, establishing very early the singularity of a clade of benthic species (including *P. concavum*, *P. hoffmannianum* or *P. lima*) with the symmetrical contour of the lateral plates (Grzebyk et al., 1998; Murray et al., 2009; Hoppenrath et al., 2013; Boopathi et al., 2015; Chomérat et al., 2019; this study, Fig. 7). The other species, which generally exhibit an asymmetric component in their morphology, are distributed across various clades and subclades within the genus, the number of which increased as the number of species analyzed increased (Hoppenrath et al., 2013; Chomérat et al., 2019).

The clade formed of *P. venetum* with *P. triestinum* and *P. redfieldii* is strongly supported despite the conspicuous difference in cell shape, with an approximately oval shape in *P. venetum* as opposed to a lanceolate shape with a more distinctly pointed posterior end in the other two species. The proximity of oval shape species with species with a pointed posterior end is also observed in the sister clade encompassing *P. micans*, with *P. rhathymum* and *P. steidingerae* on one hand, and *P. micans*, *P. gracile* and *P. koreanum* on the other hand (Fig. 7). In the *Prorocentrum* phylogenetic tree (Fig. 7), basal clades and taxa mostly show a thecal plate shape with a rounded posterior end whereas the *P. triestinum* and

P. micans clades appear to be among the most recently diverged in the genus, suggesting that the pointed posterior end was a late-emerging feature in the genus. The variation in the shape of posterior end between the two varieties described in *P. texanum* within the *P. micans* clade (Henrichs et al., 2013), one with a rounded posterior end (var. *texanum*) and the other with a pointed posterior end (var. *cuspidatum*), appears to be some kind of vestigial mark of the evolutionary emergence of the morphological transition of the posterior end in this branch of the genus *Prorocentrum*.

Changes in the number and distribution of large pores also appear to reflect an evolutionary pattern in the two sister clades. The higher number of large pores of *P. venetum* in its clade is partly due to the two radial rows of pores. Similarly, in the clade encompassing *P. micans*, radial rows of large pores (between 2 and 6 pairs depending on taxa) contribute to a generally higher number of pores. Thus, the reduction in the number of large pores (especially those arranged in rows) appears to be an evolutionarily derived feature in this branch of the genus *Prorocentrum*. Altogether, thecal plates of *P. venetum* seem to have retained more ancestral features as compared to *P. triestinum* and *P. redfieldii*.

The phylogenetic analyses of the three considered rDNA regions (Supplementary Figs. S6-S8) provided different metric scales that appeared differently useful for the genetic delimitation of related *Prorocentrum* species. The few units of nucleotide substitutions on these rDNA regions may be sufficient to separate sister clades or species, however, relationships between species clades were not always well resolved. Besides for some species clades, genetic variability carried by a similar number of substitutions, may suggest internal subclades or peripheral clades possibly representing cryptic species. In the analysis with the three combined rDNA regions (18S–D3 analysis, Fig. 7, Supplementary Figs. S4-S5), the delimitation of species and the resolution of relationships between species appeared to have been improved within the genus *Prorocentrum*, despite the small number of such data available to date (especially those obtained in the form of fully assembled sequences).

5. Conclusions

The morphological description of *P. venetum* is complemented with fine detail on thecal plate morphology and periflagellar platelets. The phylogenetic analysis demonstrated that *P. venetum* belongs to the same lineage as *P. triestinum* and *P. redfieldii*. Morphologically, this lineage can be defined by several synapomorphic characters including the significant size-reduction of the accessory pore and the adjacent platelet 7, and the presence of a row of large pores along the dorsal edge of the posterior end of both thecal plates. Both morphologically and phylogenetically, *P. venetum* is not a synonym of *P. mexicanum*, contrary to what was suggested in Gómez et al. (2017), and this is consistent with the description of this organism as a distinct species by Tolomio and Cavolo (1985).

CRediT authorship contribution statement

Daniel Grzebyk: Writing – original draft, Methodology, Investigation, Formal analysis, Data curation, Conceptualization. **Mona Hoppenrath:** Writing – original draft, Methodology, Investigation, Formal analysis, Conceptualization. **Urban Tillmann:** Writing – original draft, Methodology, Investigation, Formal analysis, Conceptualization.

Author agreement

All authors have seen and approved the final version of the manuscript being submitted. The article is the authors' original work, it hasn't received prior publication and isn't under consideration for publication elsewhere.

Declaration of competing interest

The authors declare the following financial interests/personal relationships which may be considered as potential competing interests: Daniel Grzebyk reports equipment, drugs, or supplies was provided by LabEx CeMEB. If there are other authors, they declare that they have no known competing financial interests or personal relationships that could have appeared to influence the work reported in this paper.

Acknowledgements

The genetic work was carried out with the support of LabEx CeMEB, an ANR 'Investissement d'Avenir' programme (ANR-10-LABX-04-01), through the use of the GenSeq sequencing facility. Thanks to C. Mestres for assistance in the genetic analysis during a technical internship. MH thanks F. Iwan (Senckenberg am Meer, DZMB) for TEM work.

Appendix A. Supplementary data

Supplementary data to this article can be found online at https://doi.org/10.1016/j.protis.2025.126099.

References

Altschul, S.F., Gish, W., Miller, W., Myers, E.W., Lipman, D.J., 1990. Basic local alignment search tool. J. Molec. Biol. 215, 403–410. https://doi.org/10.1016/S0022-2836(05)80360-2.

Andersen, R.A., 2005. Algal culturing techniques. Academic Press, p. 578.

Anisimova, M., Gascuel, O., 2006. Approximate likelihood-ratio test for branches: a fast, accurate, and powerful alternative. Syst. Biol. 55, 539–552. https://doi.org/10.1080/10635150600755453.

Arteaga-Sogamoso, E., Rodríguez, F., Amato, A., Ben-Gigirey, B., Fraga, S., Mafra, L.L., Fernandes, L.F., de Azevedo Tibiriçá, C.E.J., Chomérat, N., Nishimura, T., Homma, C., Adachi, M., Mancera-Pineda, J.E., 2023. Morphology and phylogeny of *Prorocentrum porosum* sp. nov. (Dinophyceae): a new benthic toxic dinoflagellate from the Atlantic and Pacific Oceans. Harmful Algae 121, 102356. https://doi.org/10.1016/j.hal.2022.102356.

Bec, B., Collos, Y., Souchu, P., Vaquer, A., Lautier, J., Fiandrino, A., Benau, L., Orsoni, V., Laugier, T., 2011. Distribution of picophytoplankton and nanophytoplankton along an anthropogenic eutrophication gradient in French Mediterranean coastal lagoons. Aquat. Microb. Ecol. 63, 29–45. https://doi.org/10.3354/ame01480.

Bergh, R.S., 1881. Der Organismus der Cilioflagellaten. Eine Phylogenetische Studie. Morphologisches Jahrbuch 7, 177–288, pl. 12–16.

Bernardi Aubry, F., Acri, F., Finotto, S., Pugnetti, A., 2021. Phytoplankton dynamics and water quality in the Venice Lagoon. Water 13, 2780. https://doi.org/10.3390/w13192780.

Boopathi, T., Faria, D.G., Cheon, J.-Y., Youn, S.H., Ki, J.-S., 2015. Implications of high molecular divergence of nuclear rRNA and phylogenetic structure for the dinoflagellate *Prorocentrum* (Dinophyceae, Prorocentrales). J. Eukaryot. Microbiol. 62, 519–531. https://doi.org/10.1111/jeu.12206.

Bursa, A., 1959. The genus *Prorocentrum* Ehrenberg. Morphodynamics, protoplasmatic structures, and taxonomy. Can. J. Bot. 37, 1–31. https://doi.org/10.1139/b59-001.

Bursa, A.S., 1962. Some morphogenetic factors in taxonomy of dinoflagellates. Grana Palynol. 3, 54–66. https://doi.org/10.1080/00173136209429104.

Chomérat, N., Gatti, C.M.I., Nézan, E., Chinain, M., 2017. Studies on the benthic genus *Sinophysis* (Dinophysales, Dinophyceae) II. *S. canaliculata* from Rapa Island (French Polynesia). Phycologia 56, 193–203. https://doi.org/10.2216/16-24.1.

Chomérat, N., Bilien, G., Zentz, F., 2019. A taxonomical study of benthic *Prorocentrum* species (Prorocentrales, Dinophyceae) from Anse Dufour (Martinique Island, eastern Caribbean Sea). Mar. Biodivers. 49, 1299–1319. https://doi.org/10.1007/s12526-018-0913-6.

Cohen-Fernandez, E.J., Meave Del Castillo, E., Salgado Ugarte, I.H., Pedroche, F.F., 2006. Contribution of external morphology in solving a species complex: the case of *Prorocentrum micans*, *Prorocentrum gracile* and *Prorocentrum sigmoides* (Dinoflagellata) from the Mexican Pacific Coast. Phycol. Res. 54, 330–340. https://doi.org/10.1111/j.1440-1835.2006.00440.x.

David, H., Laza-Martínez, A., García-Etxebarria, K., Riobó, P., Orive, E., 2014. Characterization of *Prorocentrum elegans* and *Prorocentrum levis* (Dinophyceae) from the southeastern Bay of Biscay by morphology and molecular phylogeny. J. Phycol. 50, 718–726. https://doi.org/10.1111/jpy.12200.

Dereeper, A., Guignon, V., Blanc, G., Audic, S., Buffet, S., Chevenet, F., Dufayard, J.F., Guindon, S., Lefort, V., Lescot, M., Claverie, J.M., Gascuel, O., 2008. Phylogeny.fr: robust phylogenetic analysis for the non-specialist. Nucleic Acids Res. 36, W465–W469. https://doi.org/10.1093/nar/gkn180.

Dodge, J.D., Crawford, R.M., 1971. A fine-structural survey of dinoflagellate pyrenoids and food-reserves. Bot. J. Linn. Soc. 64, 105–115. https://doi.org/10.1111/j.1095-8339.1971.tb02138.x.

Ehrenberg, C.G., 1834. Dritter Beitrag zur Erkenntnis großer Organisation in der Richtung des kleinsten Raumes. Abhandlungen der Physikalisch-Mathematischen Klasse der Königlichen Akademie der Wissenschaften zu Berlin 1833, 145–336.
Faust, M.A., 1990. Morphologic details of six benthic species of *Prorocentrum* (Pyrrophyta) from a mangrove island, Twin Cays, Belize, including two new species. J. Phycol. 26, 548–558. https://doi.org/10.1111/j.0022-3646.1990.00548.x.
Faust, M.A., 1993. *Prorocentum belizeanum*, *Prorocentrum elegans*, and *Prorocentrum caribbaeum*, three new benthic species (Dinophyceae) from a mangrove island, Twin Cays, Belize. J. Phycol. 29, 100–107. https://doi.org/10.1111/j.1529-8817.1993.tb00287.x.
Fensome, R.A., Taylor, F.J.R., Norris, G., Sarjeant, W.A.S., Wharton, D.I., Williams, G.L., 1993. A classification of living and fossil dinoflagellates. Micropaleontology. Spec. Publ. 7, 1–351.
Gómez, F., 2008. Phytoplankton invasions: comments on the validity of categorizing the non-indigenous dinoflagellates and diatoms in European Seas. Mar. Poll. Bull. 56, 620–628. https://doi.org/10.1016/j.marpolbul.2007.12.014.
Gómez, F., Qiu, D., Lin, S., 2017. The synonymy of the toxic dinoflagellates *Prorocentrum mexicanum* and *P. rhathymum* and the description of *P. steidingerae* sp. nov. (Prorocentrales, Dinophyceae). J. Eukaryot. Microbiol. 64, 668–677. https://doi.org/10.1111/jeu.12403.
Gómez, F., Gourvil, P., Li, T., Huang, Y., Zhang, H., Courcot, L., Artigas, L.F., Soler Onís, E., Gutiérrez-Rodríguez, A., Lin, S., 2023. Molecular phylogeny of the spiny-surfaced species of the dinoflagellate *Prorocentrum* with the description of *P. thermophilum* sp. nov. and *P. criophilum* sp. nov. (Prorocentrales, Dinophyceae). J. Phycol. 59, 70–86. https://doi.org/10.1111/jpy.13298.
Gourret, P., 1883. Les Péridiniens du Golfe de Marseille. Annales Mus. Hist. Nat. Marseille (Zool.) 1, 1–114.
Grzebyk, D., Sako, Y., Berland, B., 1998. Phylogenetic analysis of nine species of *Prorocentrum* (Dinophyceae) inferred from 18S ribosomal DNA sequences, morphological comparisons, and description of *Prorocentrum panamensis*, sp. nov. J. Phycol. 34, 1055–1068. https://doi.org/10.1046/j.1529-8817.1998.341055.x.
Grzebyk, D., Audic, S., Lasserre, B., Abadie, E., de Vargas, C., Bec, B., 2017. Insights into the harmful algal flora in northwestern Mediterranean coastal lagoons revealed by pyrosequencing metabarcodes of the 28S rRNA gene. Harmful Algae 68, 1–16. https://doi.org/10.1016/j.hal.2017.06.003.
Grzebyk, D., Pasqualini, V., Garrido, M., Quilichini, Y., Pereto, C., Cecchi, P., 2022. Insight into the morphology and genetic diversity of the *Chaetoceros tenuissimus* (Bacillariophyta) species complex. Eur. J. Phycol. 57, 507–525. https://doi.org/10.1080/09670262.2022.2029949.
Guindon, S., Dufayard, J.F., Lefort, V., Anisimova, M., Hordijk, W., Gascuel, O., 2010. New algorithms and methods to estimate maximum-likelihood phylogenies: assessing the performance of PhyML 3.0. Syst. Biol. 59, 307–321. https://doi.org/10.1093/sysbio/syq010.
Guiry, M.D., 2022. *Prorocentrum venetum* Tolomio & Cavolo 1985. In: Guiry, M.D., Guiry, G.M. (Eds.), *AlgaeBase*, World-Wide Electronic Publication. National University of Ireland, Galway. http://www.algaebase.org (accessed 24 November 2022).
Hall, T.A., 1999. BioEdit: a user-friendly biological sequence alignment editor and analysis program for Windows 95/98/NT. Nucleic Acids Symp. Ser. 41, 95–98.
Han, M.-S., Wang, P., Kim, J.H., Cho, S.-Y., Park, B.S., Kim, J.-H., Katano, T., Kim, B.-H., 2016. Morphological and molecular phylogenetic position of *Prorocentrum micans* sensu stricto and description of *Prorocentrum koreanum* sp. nov. from Southern coastal waters in Korea and Japan. Protist 167, 32–50. https://doi.org/10.1016/j.protis.2015.12.001.
Henrichs, D.W., Scott, P.S., Steidinger, K.A., Errera, R.M., Abraham, A., Campbell, L., 2013. Morphology and phylogeny of *Prorocentrum texanum* sp. nov. (Dinophyceae): a new toxic dinoflagellate from the Gulf of Mexico coastal waters exhibiting two distinct morphologies. J. Phycol. 49, 143–155. https://doi.org/10.1111/jpy.12030.
Hoppenrath, M., Chomérat, N., Horiguchi, T., Schweikert, M., Nagahama, Y., Murray, S., 2013. Taxonomy and phylogeny of the benthic *Prorocentrum* species (Dinophyceae)—a proposal and review. Harmful Algae 27, 1–28. https://doi.org/10.1016/j.hal.2013.03.006.
Huelsenbeck, J.P., Ronquist, F., 2001. MRBAYES: Bayesian inference of phylogenetic trees. Bioinformatics 17, 754–755. https://doi.org/10.1093/bioinformatics/17.8.754.
Hulburt, E.M., 1965. Three closely allied dinoflagellates. J. Phycol. 1, 95–96. https://doi.org/10.1111/j.1529-8817.1965.tb04564.x.
Johnson, M., Zaretskaya, I., Raytselis, Y., Merezhuk, Y., McGinnis, S., Madden, T.L., 2008. NCBI BLAST: a better web interface. Nucleic Acids Res. 36, W5–W9. https://doi.org/10.1093/nar/gkn201.
Kowallik, K., 1969. The crystal lattice of the pyrenoid matrix of *Prorocentrum micans*. J. Cell Sci. 5, 251–269. https://doi.org/10.1242/jcs.5.1.251.
Larkin, M.A., Blackshields, G., Brown, N.P., Chenna, R., McGettigan, P.A., McWilliam, H., Valentin, F., Wallace, I.M., Wilm, A., Lopez, R., Thompson, J.D., Gibson, T.J., Higgins, D.G., 2007. Clustal W and Clustal X version 2.0. Bioinformatics 23, 2947–2948. https://doi.org/10.1093/bioinformatics/btm404.
Lefort, V., Longueville, J.-E., Gascuel, O., 2017. SMS: Smart Model Selection in PhyML. Mol. Biol. Evol. 34, 2422–2424. https://doi.org/10.1093/molbev/msx149.
Lemoine, F., Correia, D., Lefort, V., Doppelt-Azeroual, O., Mareuil, F., Cohen-Boulakia, S., Gascuel, O., 2019. NGPhylogeny.fr: new generation phylogenetic services for non-specialists. Nucleic Acids Res. 47, W260–W265. https://doi.org/10.1093/nar/gkz303.
Lim, A.S., Jeong, H.J., Jang, T.Y., Kang, N.S., Lee, S.Y., Yoo, Y.D., Kim, H.S., 2013. Morphology and molecular characterization of the epiphytic dinoflagellate *Prorocentrum* cf. *rhathymum* in temperate waters off Jeju Island, Korea. Ocean Sci. J. 48, 1–17. https://doi.org/10.1007/s12601-013-0001-6.
Loeblich III, A.R., Sherley, J.L., Schmidt, R.J., 1979. The correct position of flagellar insertion in *Prorocentrum* and description of *Prorocentrum rhathymum* sp. nov. (Pyrrhophyta). J. Plankton Res. 1, 113–120. https://doi.org/10.1093/plankt/1.2.113.
Murray, S., Nagahama, Y., Fukuyo, Y., 2007. Phylogenetic study of benthic, spine-bearing prorocentroids, including *Prorocentrum fukuyoi* sp. nov. Phycol. Res. 55, 91–102. https://doi.org/10.1111/j.1440-1835.2007.00452.x.
Murray, S., Ip, C.L.C., Moore, R., Nagahama, Y., Fukuyo, Y., 2009. Are prorocentroid dinoflagellates monophyletic? A study of 25 species based on nuclear and mitochondrial genes. Protist 160, 245–264. https://doi.org/10.1016/j.protis.2008.12.004.
Ndhlovu, A., Dhar, N., Garg, N., Xuma, T., Pitcher, G.C., Sym, S.D., Durand, P.M., 2017. A red tide forming dinoflagellate *Prorocentrum triestinum*: identification, phylogeny and impacts on St Helena Bay, South Africa. Phycologia 56, 649–665. https://doi.org/10.2216/16-114.1.
Osorio Tafall, B.F., 1942. Notas sobre dinoflagelados planctónicos marinos de México, con descripción de nuevas especies. Anal. Esc. Nal. Cien. Biol. Méx. 2, 435–447 (Lám. 34-36).
Pei, L., Hu, W., Wang, P., Kang, J., Mohamed, H.F., Wang, C., Liu, L., Luo, Z., 2022. Morphologic and phylogenic characterization of two bloom-forming planktonic *Prorocentrum* (Dinophyceae) species and their potential distribution in the China Sea. Algal Res. 66, 102788. https://doi.org/10.1016/j.algal.2022.102788.
Schiller, J., 1918. Über neue *Prorocentrum*– und *Exuviaella*–Arten aus der Adria. Arch. Protistenkd. 38, 250–262.
Schiller, J., 1928. Die plaktische vegetationen des Adriatischen Meeres. C. Dinoflagellata I Teil. Adiniferidae, Dinophysidaceae. Arch. Protistenkd. 61, 46–91.
Schiller, J., 1933. Dinoflagellatae (Peridineae) in monographischer Behandlung. In: Kolkwitz, R. (Ed.), L. Rabenhorst's Kryptogamen–Flora von Deutschland, Österreich und der Schweiz. Zehnter band Flagellatae. Akademische Verlagsgesellschaft, Leipzig, p. 615.
Skejić, S., Car, A., Marasović, I., Jozić, S., Bužančić, M., Arapov, J., Ninčević Gladan, Ž., Bakrač, A., Kušpilić, G., Vidjac, O., Larsen, J., 2017. Morphology and ecology of the poorly known dinoflagellate *Prorocentrum arcuatum* (Dinophyceae) from the Medulin Bay (eastern Adriatic Sea). Acta Adriat. 58, 41–52. https://doi.org/10.32582/aa.58.1.3.
Stein, F., 1883. Der Organismus der Infusionsthiere nach eigenen Forschungen in systematischer Reihenfolge bearbeitet. III. Abt. II. Hälfte. In: Der Organismus der Arthrodelen Flagellaten, W. Engelmann, Leipzig, p. 30.
Taylor, F.J.R., 1980. On dinoflagellate evolution. Biosystems 13, 65–108. https://doi.org/10.1016/0303-2647(80)90006-4.
Thessen, A.E., Patterson, D.J., Murray, S.A., 2012. The taxonomic significance of species that have only been observed once: the genus *Gymnodinium* (Dinoflagellata) as an example. PloS One 7, e44015. https://doi.org/10.1371/journal.pone.0044015.
Tillmann, U., Hoppenrath, M., Gottschling, M., 2019. Reliable determination of *Prorocentrum micans* Ehrenb. (Prorocentrales, Dinophyceae) based on newly collected material from the type locality. Eur. J. Phycol. 54, 417–431. https://doi.org/10.1080/09670262.2019.1579925.
Tillmann, U., Beran, A., Gottschling, M., Wietkamp, S., Hoppenrath, M., 2022. Clarifying confusion – *Prorocentrum triestinum* J.Schiller and *Prorocentrum redfieldii* Bursa (Prorocentrales, Dinophyceae) are two different species. Eur. J. Phycol. 57, 207–226. https://doi.org/10.1080/09670262.2021.1948614.
Tillmann, U., Gottschling, M., Wietkamp, S., Hoppenrath, M., 2023a. Morphological and phylogenetic characterisation of *Prorocentrum spinulentum*, sp. nov. (Prorocentrales, Dinophyceae), a small spiny species from the North Atlantic. Microorganisms 11, 271. https://doi.org/10.3390/microorganisms11020271.
Tillmann, U., Wietkamp, S., Gottschling, M., Hoppenrath, M., 2023b. *Prorocentrum pervagatum* sp. nov. (Prorocentrales, Dinophyceae): a new, small, planktonic species with a global distribution. Phycol. Res. 71, 56–71. https://doi.org/10.1111/pre.12502.
Tolomio, C., 1988. Observations taxinomiques et ultrastructurales sur des exemplaires de *Prorocentrum* (Dinophyceae) récoltés dans les eaux côtières de la Corse du Sud-Est. Bot. Mar. 31, 223–230. https://doi.org/10.1515/botm.1988.31.3.223.
Tolomio, C., Cavolo, F., 1985. Description de *Prorocentrum venetum* sp. nov. (Dinophyceae) trouvé dans la Lagune de Venise. Bot. Mar. 28, 345–350. https://doi.org/10.1515/botm.1985.28.8.345.
Zhang, H., Li, Y., Cen, J., Wang, H., Cui, L., Dong, Y., Lu, S., 2015. Morphotypes of *Prorocentrum lima* (Dinophyceae) from Hainan Island, South China Sea: morphological and molecular characterization. Phycologia 54, 503–516. https://doi.org/10.2216/15-8.1.